

# Design optimisation of an impeller with CFD and Meta-Model of optimal Prognosis (MoP)

**Florian Frese**

Voith Turbo Aufladungssysteme, Germany

**Johannes Einzinger**

ANSYS, Germany

**Johannes Will**

Dynardo , Germany

## Abstract

The CFD method is used to predict the flow and the compressor map. For the optimisation CAE-based parametric optimisation with respect to 15 geometry parameters, based on the primary design is used. The optimisation procedure is divided in two steps:

The first one is the sensitivity study combined with the generation of the Metamodel of optimal Prognosis (MoP), where the most relevant input parameters and a quality assurance of the model could be identified. In addition the MoP can be used for optimisation to predict the performance of the compressor in the whole parameter space and to search for optimal designs.

The second step, for further design improvement, is an optimisation procedure using additional solver calls, where the ARSM (Adaptive Response Surface Method) algorithm is selected for optimisation. The subdomain of important parameter is defined with respect to the result of the MoP.

The whole optimisation strategy is designed to work in large parameter spaces (>10..100) with a minimum number of CFD simulations, "no run too much"; to find an improved design.

## Nomenclature

b	blade thickness	L	blade length
m	mass flow	u	circumferential velocity
N	node		

## Greek Letters

$\beta$	blade angle	$\Theta$	temperature
$\eta$	efficiency	$\Pi$	pressure ratio

## Subscripts

1.0	compressor inlet	ini	initial design
1.1	rotor outlet	is	isentropic
1.2	diffusor outlet	max	maximum
2.0	compressor outlet	n	normalized
B	blade	opt	optimised
C	compressor	T	total
CW	compressor wheel		

## 1 Introduction

At the present time the internal combustion engine is widely used for passenger cars and commercial vehicles applications. Today's newly developed combustion engines must meet five key demands. The engine should cause low costs, have a long life cycle, provide a good response with a low fuel consumption and meet the actual emission targets. To achieve these objectives, increasing of the engine power absolute and specific becomes more and more important. To fulfill the core requirements in engine development, today almost all diesel engines for commercial applications use an exhaust-gas turbocharger. During the design process, the combination of a radial turbine and a centrifugal compressor has a decisive influence on the economic operation of a combustion engine.

For matching an exhaust-gas turbocharger with an engine the performance values, such as displacement, number of cylinders, power, mass air flow, fuel consumption, boost pressure, exhaust back pressure, etc. are needed for engine design points for the target engine. Based on the performance values, at first a suitable compressor wheel and compressor housing geometry combination is selected. The compressor map (Figure 1), which is determined based on the selected compressor components is either based on measured data or as a result of numerical data, which are determined with the help of 1D and 3D-CFD programs.

The compressor map has three limitations that restrict the map width and height. These are the surge-line and the choke-line, which exist due to the aerodynamics and the maximum compressor speed  $u_{cmax}$ . The maximum compressor speed is limited by the allowable mechanical stresses in the impeller.

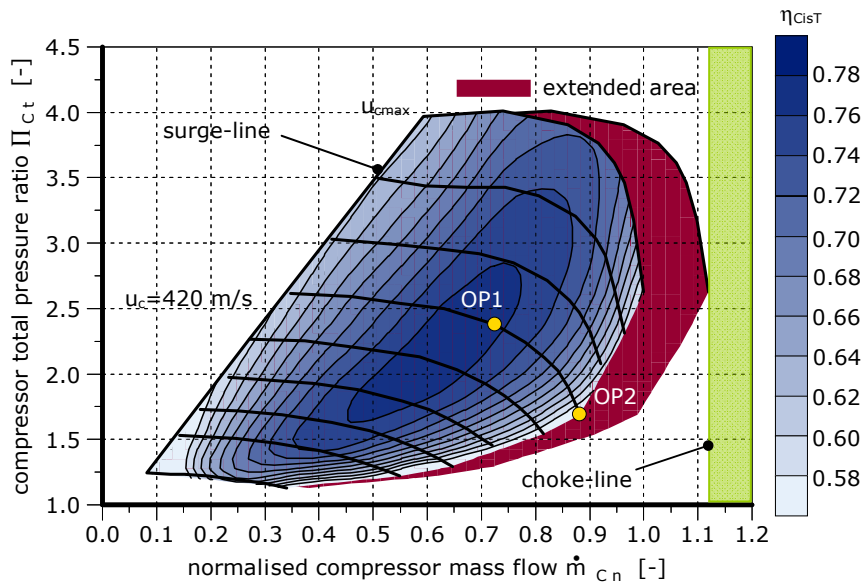


**Figure 1: compressor map with extended map range**

At the surge-line the flow tears by low mass flow and high pressure ratio that the delivering of fresh air flow is interrupted. The air mass flow run backwards through the compressor until a stable pressure ratio is reached with a positive mass flow rate, so the pressure is built up again. By periodic repeating of this procedure, the term "pump" is derived.

At the choke-line the flow reaches the speed of sound at the narrowest cross-

section at the inlet of the compressor wheel. If this condition is reached, a further increase in flow-rate is not possible even by increasing the compressor speed. All flow-curves run to the maximum flow rate value at a pressure ratio of  $\Pi_{CT}=1$ .

With the help of the identified compressor map the engine design points are investigated whether the map range of the map is sufficient. Depending on the application of the engine, a wide range of the compressor map is needed. If the map range is not adequate a new impeller has to be designed to get an extended compressor map (Figure 1) to reach the requirements.

The impeller geometry is generated by special turbo machinery design software. The redesign of the existing impeller could be done manually in which this procedure is enormous time-consuming. Another method which is presented in this paper is the automatic optimisation by numerical methods by using 3D-CFD simulations in combination with an optimiser.

## 2 Parametrical impeller geometry

For the automatic parametric optimisation the initial compressor wheel (Figure 2 a), which has seven main and seven splitter blades, needs to be parameterised.

Today the compressor wheels are milled. To guarantee such a production process impeller flank milling is required. Therefore only the blade angle of the hub and the shroud curve for the main and splitter blade are parameterised (Figure 2 b).

Figure 2 c) shows the normalised beta-angle ( $\beta_{Bn}$ ) distribution for the main blade over the normalized blade length from the leading edge to the trailing edge. The angle distribution on hub and shroud side is expressed by a Bezier-spline which is controlled by four control points (locator 1-4). During the optimisation process only the value for  $\beta_{Bn}$  is changed, for each control point, to generate a new blade design, while the location of the control point is fixed in blade length.

Each control point on the hub curve for the main blade is defined by the following equation:

$$HBPI = HBPis + DXHBi \quad i = \text{control point } 1,2,3,4. \quad (1)$$

HBPI represents during the optimisation the new normalized beta-angle at the hub contour at locator  $i$ , which is the sum of the normalized beta angle of the start design at locator  $i$  (HBPis) and the delta value of  $\beta_{Bn}$  with the control point at locator  $i$  is moved (DXHBi). The optimiser only changes the value for DXHBi.

The blade angle at the leading edge (locator 1) for a random design is described as follows:

$$0.75 = 0.8 + (-0.05)$$

The nomenclature for the control points at the shroud curve is analogue to the hub curve and defined as follows:

$$SBPI = SBPis + DXHBi \quad i = \text{control point } 1,2,3,4 \quad (2)$$

with

- SBPI = shroud at main-blade with control-point at locator  $i$
- SBPis = shroud at main-blade with control-point at locator  $i$  with start value
- DXHBi = delta value of  $\beta_{Bn}$  at main blade at locator  $i$

The locations of the Bezier-control points (1-4) on hub and shroud side are located at the same normalized blade length (0, 0.4, 0.8, and 1.0) (Figure 2 c) and

additional the parameter DXHBI is defined also on hub and shroud (equation 1 and 2). This is done to prevent an s-bend in the blade design because the blade is moved simultaneous on hub and shroud at the locator  $i$  with one value expressed by DXBi, which is mentioned above the input parameter for the optimiser.

The characterisation of the splitter blade is analogue to the definition mentioned above of the main blade.

During the optimisation process the blade thickness is unchanged and is exemplary shown for the main blade in Figure 2 d).

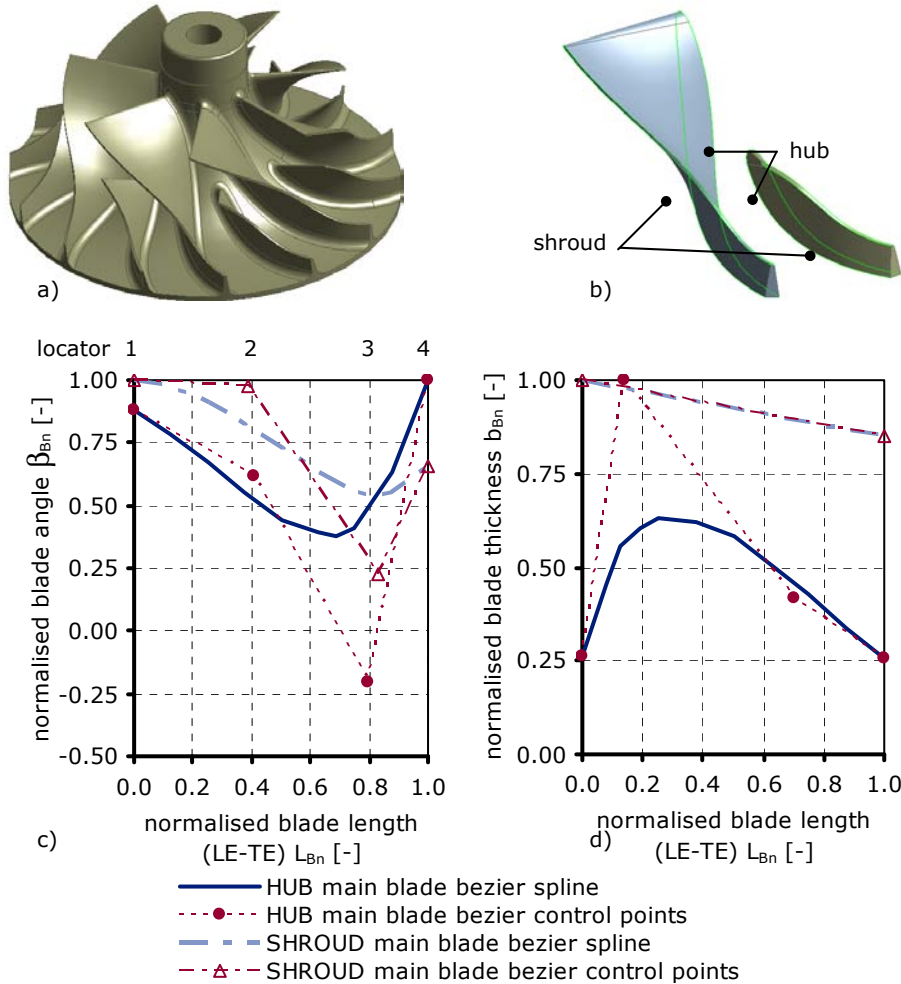


**Figure 2: a) Initial compressor; b) parametric main blade and splitter blade; c) blade angle distribution on hub and shroud for main blade; d) thickness distribution on hub and shroud for main blade**

In addition to the blades the meridian flow path is parameterised. Figure 3 shows a sketch of the flow path with the definition of the leading and trailing edge of the main and splitter blade. The locations of the leading edges of the blades are fixed, also the shroud contour because the identical compressor housing of the initial design should be used.

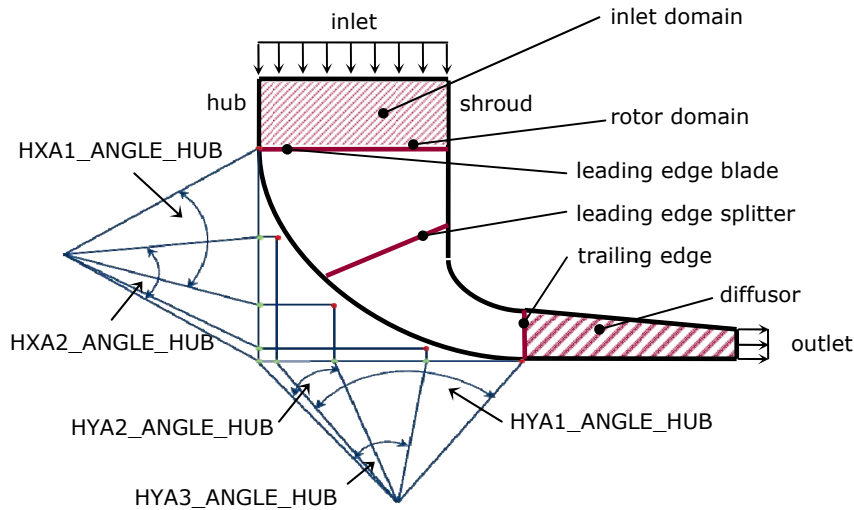


**Figure 3: Parametric meridian flow path**

Here the compressor wheel is milled and therefore the hub contour could be modified. This contour is parameterised with five angle parameters which are controlling the base points of the spline which describe the hub contour (Figure 3). In summary the compressor model is build up with 13 parameters:

- eight parameters for the beta-distribution (four @ main blade and four @ splitter blade)
- five parameters for the hub curve at the meridian flow path

### 3 CFD-Model

The numerical study was carried out with the CFD program ANSYS CFX 13.0. In the present paper two different models were investigated. One model is a complete compressor stage (Figure 4 b) consists of:

- inlet domain
- rotor domain
- diffuser domain
- volute domain
- outlet domain.

A full model is not applicable for an optimisation and therefore a periodic segment of 360/7 degree (Figure 3 and Figure 4 a) is used which includes only the

- inlet domain
- rotor domain
- diffuser domain.

For the inlet, rotor, diffuser and outlet domain a hexahedral mesh was used. Because of the geometric complexity a unstructured tetrahedral and prism mesh was used for the volute.

The physical and numerical setup for both models is equal and is defined as follows:

- inlet: total pressure and total temperature (flow direction: normal to boundary)
- outlet: mass flow
- rotor: angular velocity
- wall: adiabatic
- rotor stator interface: frozen rotor
- numeric: SST-turbulence model, second order discretisation
- 

The periodic segment uses additional a periodic condition boundary for the periodic faces (Figure 4 a).

Before the optimisation starts a grid study for the rotor was done to investigate the influence of the mesh density regarding the results. Therefore the periodic model was used with four different mesh sizes and two different advection schemes (up wind and high resolution). An overview of the grid study is shown in Table 1.

**Table 1: Overview of rotor grid study**

		Grid 1		Grid 2		Grid 3		Grid 4	
N	[-]	674878		1366156		2744902		5113334	
		High Res.	Up Wind						
$u_c$	[m/s]	420	420	420	420	420	420	420	420
$m_c$	[kg/s]	0.275	0.275	0.275	0.275	0.275	0.275	0.275	0.275
$\Pi_{CWT}$	[-]	0.818	0.782	0.826	0.802	0.826	0.803	0.828	0.814
$\eta_{CWisT}$	[-]	2.361	2.339	2.374	2.371	2.375	2.356	2.379	2.375

As an evaluation criterion the total pressure ratio ( $\Pi_{CWT}$ ) and the total isentropic efficiency ( $\eta_{CWisT}$ ) for the compressor wheel and the diffuser was used. The total compressor ratio

$$\Pi_{CWT} = \frac{p_{T1.2}}{p_{T1.0}} \quad (5)$$

is formed by the total pressure at diffuser outlet  $p_{T2.0}$  divided by the total pressure at compressor inlet  $p_{T1.0}$ . The compressor wheel efficiency is calculated by

$$\eta_{CWisT} = \frac{\left(\Pi_{CWT}\right)^{\frac{\kappa-1}{\kappa}}}{\left[\left(\frac{T_{T1.2}}{T_{T1.0}}\right) - 1\right]} \quad (6)$$

with  $\kappa$  as the isentropic coefficient for air, the total temperature at diffuser outlet  $T_{T1.2}$  and the total temperature at compressor inlet  $T_{T1.0}$ . The grid study has shown that the Grid 2 is a good compromise between numerical accuracy and computational time and will be used for the optimisation study. Following the grid study the full model with a resolution of 12 million nodes was used to estimate the deviation between the test data and numerical results for the initial compressor stage. For the comparison the total pressure ratio and the total isentropic compressor efficiency for the full stage follows equation (5) and (6) was used whereby the pressure and temperature for diffuser outlet was replaced by the quantities at compressor outlet (Figure 4 b). Figure 4 c) and d) show the comparison between the measured and simulated data by a compressor speed  $u_c=420\text{m/s}$  with a satisfying accuracy.

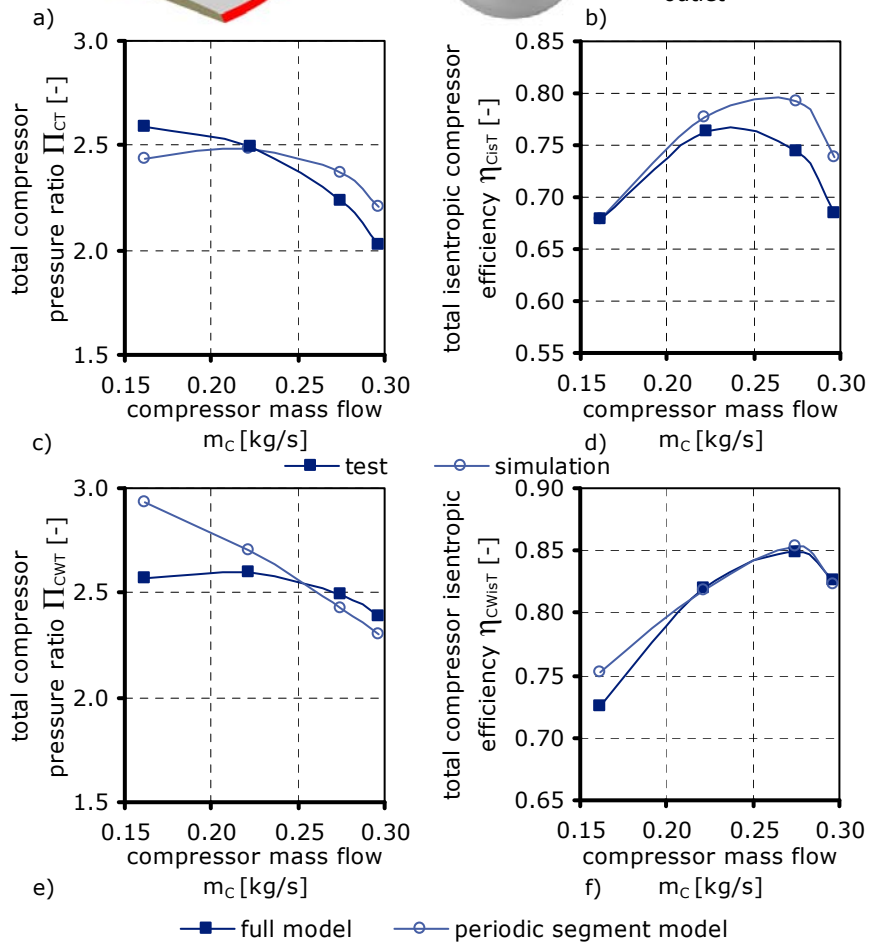
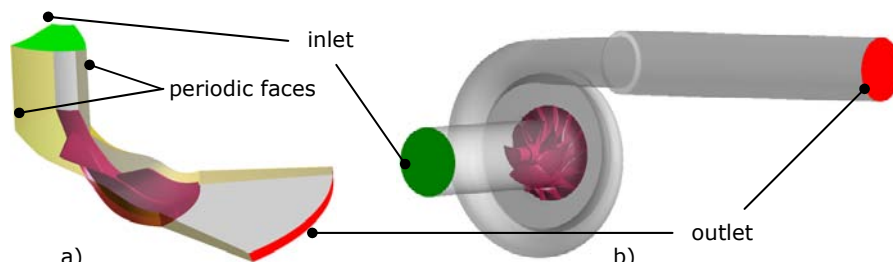


**Figure 4: a) CFD-Model periodic segment; b) CFD-model full model; c) comparison  $\Pi_{CT}$  @  $u_c=420m/s$ : test vs. CFD-simulation full model; d) comparison  $\eta_{CisT}$  @  $u_c=420m/s$ : test vs. CFD-simulation full model; e) comparison  $\Pi_{CWT}$  @  $u_c=420m/s$ : CFD-simulation full model vs. CFD-simulation periodic segment; f) comparison  $\eta_{CwisT}$  @  $420m/s$ : CFD-simulation full model vs. CFD-simulation periodic segment**

For assessment the numerical error for the periodic segment the pressure ratio and the compressor efficiency was compared to the full model and is shown in Figure 4 f). Only a difference at the surge line could be seen, because of flow separation.

For the optimisation two operating points (OP) are considered (Figure 1):

- OP1:  $u_c = 420\text{m/s}$ ;  $m_{cn} = 0.73$ ;  $\Pi_{CT} = 2.37$
- OP2:  $u_c = 420\text{m/s}$ ;  $m_{cn} = 0.88$ ;  $\Pi_{CT} = 1.68$

#### 4 Optimisation

The optimisation procedure is carried out in three steps:

1. In step one a sensitivity analysis is performed in order to determine the most important design variables. This is realized with help of the Meta-model of Optimal Prognosis (MOP, see Most and Will [1]).
2. Using the MOP a response surface-based optimisation is carried out next. For this procedure the search for the optimum requires no direct solver runs. The determined optimum is verified finally with only a single solver call. Considering the results of the sensitivity analysis, only the most important input variables are used as design parameters within this procedure.
3. Using the results of step two as basis, now an optimisation is performed by using direct solver calls.

Some remarks concerning the sensitivity analysis:

In order to analyze the influence of the input parameters on a certain response parameter, global variance-based sensitivity measures are determined. As basis, the design space is explored with optimized Latin-Hypercube Sampling. With this stochastic sampling method, design samples are generated which cover the design space optimally by minimizing unwanted correlations between the inputs. After the generation of the samples, for each sample the solver evaluates the response values. Based on these support points in a next step an optimal approximation model is determined. This procedure, called Meta-Model of Optimal Prognosis, determines the optimal variable subspace together with the optimal approximation model, where polynomials and Moving Least Squares approximations are considered. Basis for this procedure is an objective measure to quantify the prognosis quantity of the investigated possible meta-models.

For this purpose the so-called Coefficient of Prognosis (Most and Will [2]) is utilized:

$$\text{CoP} = 1 - \frac{SS_E^{\text{Prediction}}}{SS_T} \quad (7)$$

This measure quantifies the sum of squared prediction errors with respect to data, which are not used to build up the approximation model

$$SS_E = \sum_{i=1}^N (y_i - \hat{y}_i)^2 \quad (8)$$

This non-objective error measure is scaled with the total sum of squares of the real response values

$$SS_T = \sum_{i=1}^N (y_i - \mu_Y)^2 \quad (9)$$

The optimal variables subspace is determined by applied advance filter technology as described in detail in [1]. Once the optimal subspace was found, the optimal

approximation model in this subspace is used to carry out the sensitivity analysis. Using total effect sensitivity indices, the variance contribution is quantified by the conditional output variance with respect to a single input variable (see Saltelli et al. [3])

$$S_T(X_i) = 1 - \frac{V(Y|X_i)}{V(Y)} \quad (9)$$

The sensitivity indices determined on the approximation model are finally scaled with the CoP in order to obtain the explained variation with respect to each of the considered input variables.

Applying the MOP procedure on the compressor (40 design points), see Figure 5, shows that the CoP of the total pressure ratio  $\Pi_{CWT}$  and the total temperature ratio  $\Theta_{CWT}$  is pretty high for both operation points. A value over 80% is known as a good and reliable result. Common reasons for a small value are a too small number of design points or "numerical noise" in the simulation. The "numerical noise" is reduced by the best practice study mentioned above and the monitoring of the analysis showed a stable value of the CoP. The isentropic efficiency  $\eta_{CWiSTr}$ , a more sensitive result than the other ones, has significant smaller values; i.e. we can rely to the MOP in terms of  $\Pi_{CWT}$  and  $\Theta_{CWT}$ , but we need to be careful about  $\eta_{CWiSTr}$ . Please notice, that all results are with respect to the chosen input parameters and their lower and upper limit!

The efficiency is the most important output parameter for the optimisation and this is the reason, why the MOP is not used for optimisation (It would be the fastest way!); a direct algorithm is chosen, see below.

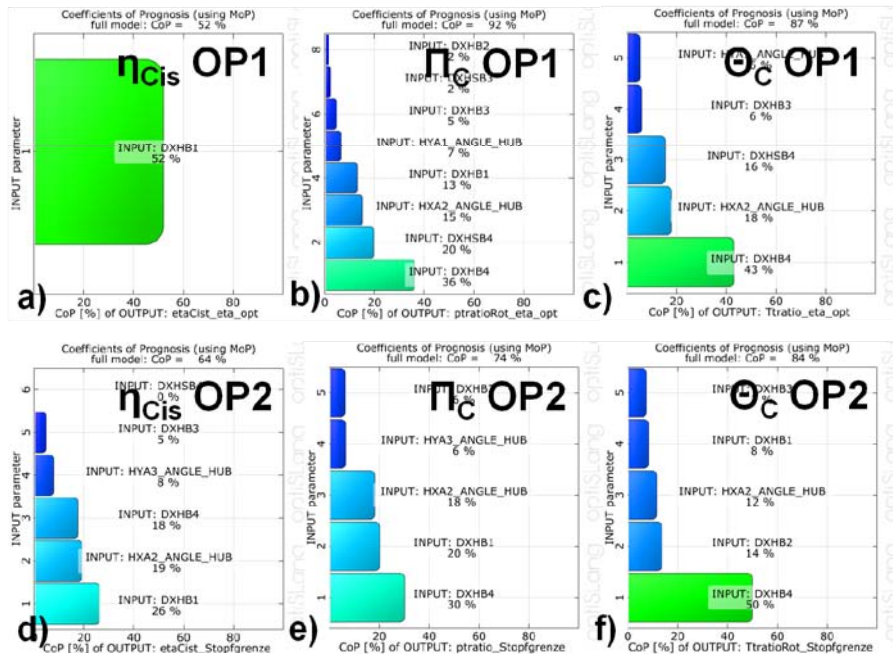


**Figure 5: Coefficient of Prognosis (CoP) and important input variables on isentropic efficiency, total pressure and temperature ratio for both operating points OP1 and OP2**

All further analysis steps are done for the relevant parameters only, which can also be seen in Figure 5. The most important variables here are:  $x_1=DXHB1$ ,  $x_2=DXHB4$  and  $x_3=HX\_A2\_ANGLE\_HUB$ . The parameters  $x_1$  and  $x_2$  manipulate the inlet and outlet angle of the main blade (Figure 2 c) and the parameter  $x_3$  manipulates the hub contour (Figure 3). Figure 6 shows the analysis, based on the Meta-model:

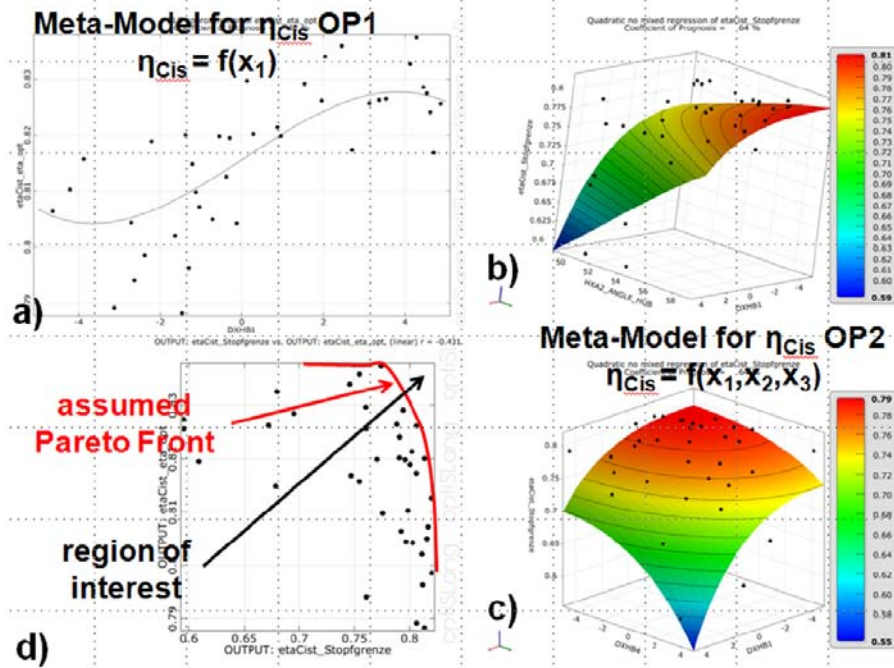


**Figure 6: Meta-model for a)  $\eta_{Cis}$  OP1 b,c)  $\eta_{Cis}$  OP2 d) Anthill plot  $\eta_{Cis}$  OP1 vs. OP2**

The isentropic efficiency of OP1 depends only on  $x_1$  Figure 6a, while at OP2 it is a function of  $x_1$ ,  $x_2$  and  $x_3$ , Figure 6b and 6c. It can be seen that a larger value of  $x_1$  would result in a better efficiency at OP1 while it would reduce the value at OP2, i.e. we have a conflict of optimisation goals. Figure 6d shows an Anthill Plot, the efficiency at OP1 vs. OP2, where one can see the assumed Pareto Front. If one chooses a certain point on the Pareto Front, one variable can only be increased by decreasing the other one.

The Sensitivity Analysis can be summarized:

1. The Meta-model is reliable, due to the CoP values of  $\Pi_{CWT}$  and  $\Theta_{CWT}$
2. A reduced set of parameters was found, 3 out of 15.
3. The Meta-model is plausible, with respect to physics

This result is the basis for the optimisation procedure: The fastest way, using the MoP directly (instead of doing numerical simulations), is not recommended, because of the small CoP of the efficiency; i.e. a direct optimisation algorithm is required. We found a Pareto conflict for the efficiency, for further resolution of this a Pareto Optimisation is required. Because these algorithms require a high number of design evaluations we did not use it in here. We resolved the conflict in terms of objectives by constraints:

- "old" objective:  $\eta_{CisT}$  OP1 = max and  $\eta_{CisT}$  OP1 = max

- “new” objective:  $\eta_{\text{CWisT}} \text{ OP1} = \max$  and  $\eta_{\text{CWisT}} \text{ OP1} > \eta_{\text{CWisT}} \text{ OP1}_{\text{ini}} - 1\%$

The new objective means, that the efficiency at OP2 should be as big as possible, while we accept a smaller one at OP1.

As Optimisation algorithm we choose the Adaptive Response Surface Algorithm (ARSM). The properties of this are:

- Finds the optimum, depending on the start point. From the Sensitivity Analysis we can see, that there is a global optimum
- Efficient for a small number of input variables (<10-15) the Sensitivity Analysis shows 3 important ones here
- Very robust algorithm

The ARSM works like that:

1. Sample the design space with a certain number of designs and solve them
2. Build a “simple” response surface and find the best point
3. Reduce the size of the design space around the best point and do next iteration, back to 1.

After 6 iterations, with 45 design evaluations we see a converged solution, see Figure 7:

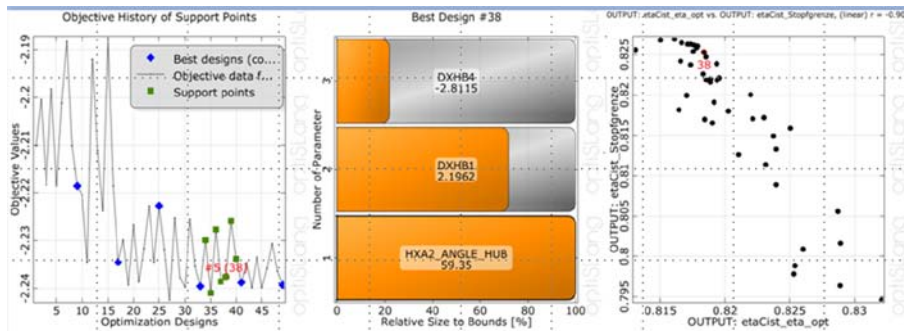


**Figure 7: Convergence of the Adaptive Response Surface Algorithm. Convergence plot of the objective function, design in parameter space and Anthill plot of evaluated designs.**

The result shows us, that  $x_2$  becomes a small, while  $x_3$  a large value; one can also see on the Meta-model. For  $x_1$ , “carrying” the conflict, we result in a medium value. The final optimized design increased the efficiency at OP2 to 2%, while 0.5% at OP1 is “lost”. Figure 7 shows also a better resolution of the Pareto conflict, because the ARSM is “driven” to the border of what is possible. Design 38 is the best in terms of the objective function, nevertheless there are other interesting designs computed.

## 5 Results

Figure 8 a) shows the measured compressor maps of the initial and optimised impeller geometry. The comparison shows that the surge-line and the speed lines below  $u_c=420$  m/s don’t deviate from the initial map. Only the speed line and therefore the total compressor pressure ratio at  $u_{c\text{max}}$  is lower than the initial one. This is caused by the backward curved main blade which reduced the maximum pressure ratio. Besides the reduced pressure ratio the flow capacity could be increased, which could be seen by the expanded flow curves above  $u_c=420$ m/s.

To reach the optimisation goals, as described in chapter **Fehler! Verweisquelle konnte nicht gefunden werden.**, the total isentropic compressor efficiency at OP1 has to be reduced to increase the flow capacity. This approach leads to efficiency lost and gain in the optimised compressor map.

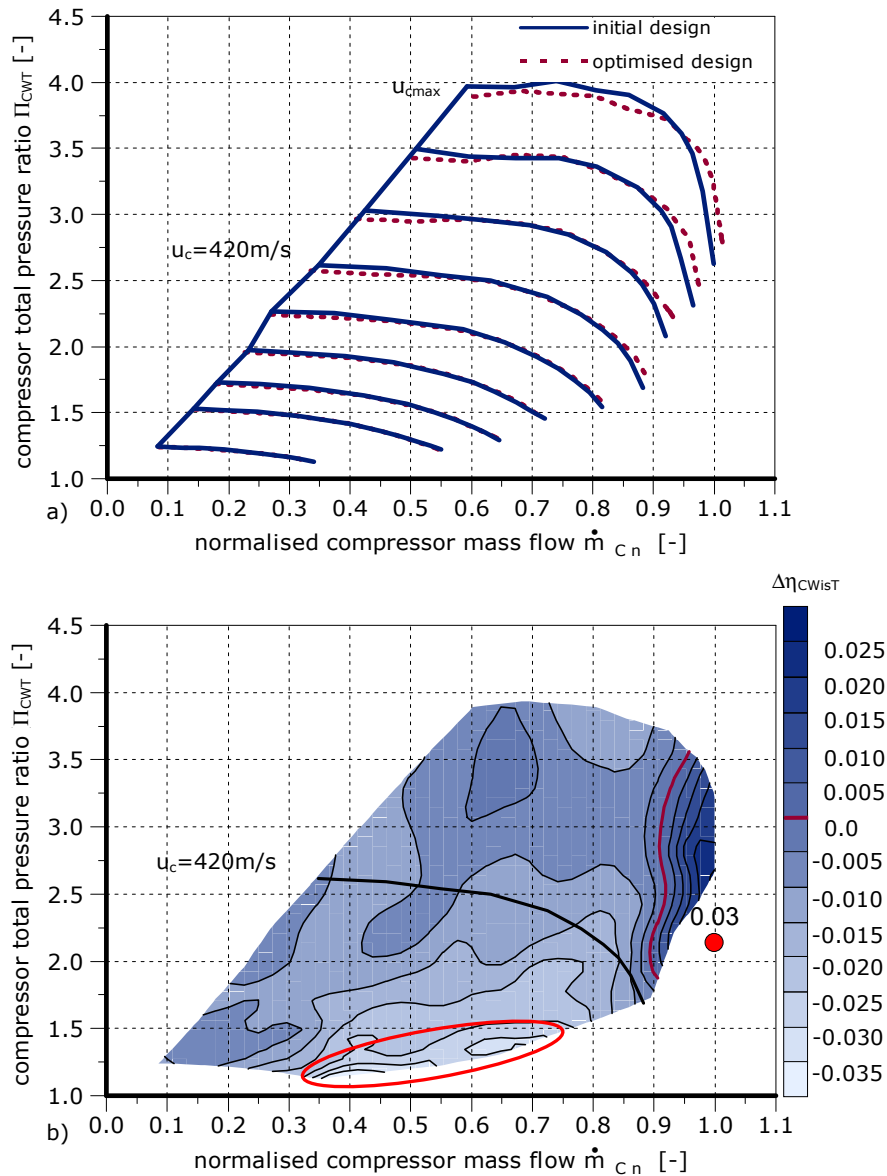


**Figure 8: Comparison of measured compressor map for initial design and optimised design: a) compressor map; b) difference in total isentropic compressor efficiency between optimised and initial design**

Therefore the delta isentropic efficiency  $\Delta\eta_{CisT}$  is used

$$\Delta\eta_{CisT} = \eta_{CisT \text{ opt}} - \eta_{CisT \text{ ini}} \quad (7)$$

which is defined by the efficiency of the optimised design  $\eta_{\text{CisT opt}}$  minus the efficiency from the initial design  $= \eta_{\text{CisT ini}}$ . Figure 8 b) shows difference map of the measured efficiency between both designs in which the map range is lower than in Figure 8 a) because only the intersection is displayed. The results show that a gain of efficiency up to 2.5% could be identified above  $m_{\text{cn}} = 0.9$  by a simultaneous reduction of the efficiency of 1.5% in the largest range of the map. Only at the lower map boundary (red ellipse Figure 8 b) the efficiency breaks down by 3.5%.

## 6 Conclusions

The optimisation of existing sub-assemblies or group of parts is always necessary for improvement. Therefore the parametric optimisation by using commercial CFD-Programs with a coupled optimiser is a useful and efficient strategy to get "fast" results.

The presented work of the impeller optimisation shows that a parametric optimisation is able to improve the design which could be confirmed by measurements. For the optimisation a parametric model of the impeller is used by 15 geometry variables. With a sensitivity study the influence of the 15 parameters are investigated regarding to the output variables total isentropic compressor efficiency and total compressor pressure ratio. With the help of the Meta-Model of optimal Prognosis (MoP) the three important design parameters are identified which are used for an adaptive-response-surface-method (ARSM) optimisation.

For the optimisation process objectives based on the sensitivity study are identified. The compressor efficiency at the operating point one has to reduce by one point of efficiency to increase the compressor efficiency and the compressor pressure ratio at operating point two.

The new impeller design shows increased flow capacity and compressor efficiency at the choke line which are defined by the objectives for the optimisation. However a slight increase in mechanical stress in the optimised impeller regarding the initial design has to be accepted.

## References

- [1] T. Most & J. Will: Metamodel of optimal prognosis - an automatic approach for variable reduction and optimal metamodel selection. Proceedings of the Weimarer Optimierungs- und Stochastiktage 5.0, Weimar, Germany, November 20-21, 2008
- [2] T. Most & J. Will: Recent advances in Meta-model of Optimal Prognosis. Proceedings of the Weimarer Optimierungs- und Stochastiktage 7.0, Weimar, Germany, October 21-22, 2010
- [3] Saltelli et al.: Global Sensitivity Analysis, The Primer. John Wiley & Sons Ltd, 2008
- [4] Dynardo GmbH: optiSLang - The Optimizing Structural Language, Version 3.2, Users Manual, 2011